

Density Functional Theory (DFT) Simulations of Shocked Liquid Xenon

Thomas R. Mattsson* and Rudolph J. Magyar†

**HEDP Theory, Sandia National Laboratories, Albuquerque, NM 87185-1189*

†*Multiscale Dynamic Material Modeling, Sandia National Laboratories, Albuquerque, NM 87185-1322*

Abstract. Xenon is not only a technologically important element used in laser technologies and jet propulsion, but it is also one of the most accessible materials in which to study the metal-insulator transition with increasing pressure. Because of its closed shell electronic configuration, Xenon is often assumed to be chemically inert, interacting almost entirely through the van der Waals interaction, and at liquid density, is typically modeled well using Leonard-Jones potentials. However, such modeling has a limited range of validity as Xenon is known to form compounds under normal conditions and likely exhibits considerably more chemistry at higher densities when hybridization of occupied orbitals becomes significant. We present DFT-MD simulations of shocked liquid Xenon with the goal of developing an improved equation of state. The calculated Hugoniot to 2 MPa compares well with available experimental shock data. Sandia is a multiprogram laboratory operated by Sandia Corporation, a Lockheed Martin Company, for the United States Department of Energy's National Nuclear Security Administration under contract DE-AC04-94AL85000.

Keywords: xenon, hugoniot, DFT, simulations

INTRODUCTION

First-principles simulations in combination with increasingly accurate shock experiments at multi-Mbar pressure have, over the last few years, yielded important insights into how matter behaves under extreme conditions. An interesting material to study under these warm dense conditions is Xenon. While under normal conditions, Xenon, consisting of closed shell atoms, is generally considered inert and well described through Lennard-Jones type potentials; there are many instances when Xenon behaves exotically. For example, Xenon has been shown to chemically bond with Fluorine and is known to become metallic under cold compression. On the other hand, it is still unknown how temperature affects this pressure-induced metallization and in detail what the Hugoniot of Xenon would be when shocked.

For many years, the cold compressed properties of Xenon have been the focus of theoretical and experimental studies. The zero temperature isotherm was calculated within $X-\alpha$ theory [2] and compares

well with shock data up to 130 kbar. Reliable gas gun data by Nellis and coworkers provides Hugoniot points up to 1.3 MBar [7]. Additional experiments and linear-muffin tin calculations were in agreement and extended the cold curve to 170 GPa [4]. Augmented plane-wave calculations were used to investigate the pressure-induced, low-temperature transition from insulator to metal, putting the critical pressure around 130 GPa and providing equation of state data to 1.3 Mbar. The insulator metal transition was further investigated using an augmented plane-wave approach with norm conserving pseudopotentials and was found to occur at about 30% compression [3]. Less extreme data for liquid xenon has been tabulated up to 350 MPa [11]. Recently, there has been diamond anvil experiments up to 80 GPa [9, 8]. The metallic like behavior of pressurized liquid xenon has been studied theoretically and experimentally [10]. A free energy model relying on chemical potentials of xenon ions has recently been used to predict the Hugoniot to ultrahigh pressures [6].

Recent theoretical work has demonstrated that

quantum molecular dynamics simulations of liquid noble Helium can provide accurate equation of state data up to high pressure regimes where path integral monte carlo becomes accurate [5]. Our work generates the Hugoniot of shocked liquid xenon to 2 MPa and compares well with available experimental shock data. The 5p-d hybridization becomes important at these high compression ratios.

COMPUTATIONAL METHOD

Central to the goal of predictive simulations in density functional theory (DFT) [12, 13] is the need for convergence [14]. The DFT-MD simulations were performed with VASP 5.1.40 [15, 16, 17], a plane-wave projector augmented-wave (PAW) core function code. [18, 19] using stringent convergence settings [14]. Steady-state simulations in the NVT ensemble used a Nosé-Hoover thermostat with velocities scaled to control temperature in the ramped-temperature simulations. Complex k-point sampling with a mean-value point $(\frac{1}{4}, \frac{1}{4}, \frac{1}{4})$ was used and is known to provide high precision for disordered structures at high temperature. Mermin’s finite temperature density functional theory [20], used here, is critical for high energy-density applications [21]. In our investigations, we had use several exchange-correlation functionals but report only the results for the generalized gradient functional, AM05 [22, 23], for simplicity. Results within the local density approximation and within other compatible generalize gradient approximations were comparable.

The main result of shock experiment is a Hugoniot curve, the set of pressure-density points achieved through varying impulses. Each point is determined by requiring that conservation of mass, momentum, and energy hold true across a shock front. Thus, the Hugoniot curve is defined with respect to a given reference state. In our instance, this reference is liquid xenon which has a molar volume 44.21 cc/mol or density of 2.97 g/cc at $T=163\text{K}$ and room pressure. With respect to the reference state, the Hugoniot condition is expressed $2(U - U_{ref}) = (P - P_{ref})(v + v_{ref})$ with U the internal energy per atom, P the system pressure, v the volume per atom, and ref designates that a value is from the unshocked reference state. In order to simulate the Hugoniot, several temperature-points for each desired density were simulated. A

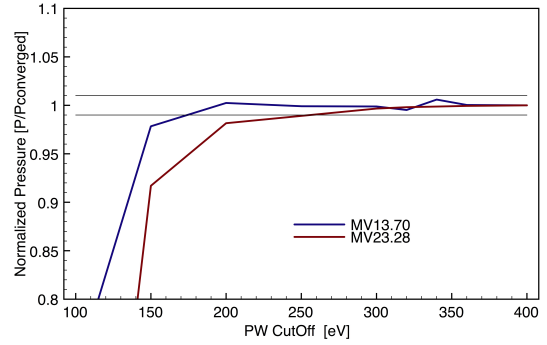


FIGURE 1. Pressure convergence with respect to the plane-wave cut-off for a 32 atom supercell of Xe within the LDA and at 10kK. MV23.28 corresponds to a density of 5.64 g/cc and MV13.70 corresponds to 9.58 g/cc. Better than 1% convergence is achieved at 300 eV cut-off.

typical fully thermalized simulation requires up to 4000 times-steps of 4 femtoseconds each.

RESULTS AND DISCUSSION

We calculated shock curves to be compared to high quality experimental data (Nellis) and frequently used equation of state models (SESAME 5190 and LEOS 540). The equation of state models diverge in the higher pressure regime of the points we considered. It was found that accurate Hugoniot curves at high temperatures were unachievable without revised 4f scattering properties in PAW potentials. Careful convergence tests and comparison to experimental results are important first steps in predictive modeling. Computationally controllable parameters such as the plane-wave cut-off should be chosen to sufficiently model the system in the sense that increasing its quality further does not affect the simulation within an desired tolerance.

In Fig. 1, we display the average pressure at 10kK for a fully thermalized run using various plane-wave cut-offs and the original pseudopotential. The run is determined to be fully thermalized when the system variables running averages do not change within a certain tolerance and the the statistical sampling size error is small enough to be below the finite basis size error. We chose a 32 atom supercell for its computational convenience but show later that this is suf-

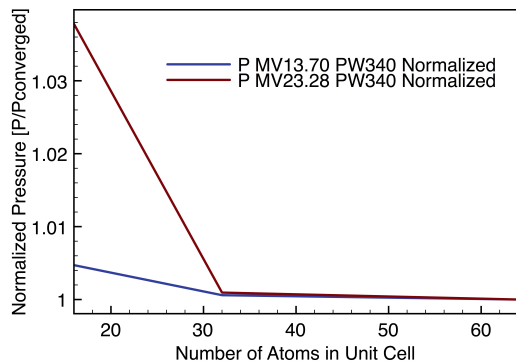


FIGURE 2. Pressure convergence with respect to the number of atoms per super cell with a 340 eV plane-wave cut-off for of Xe within the LDA. Convergence to well within 0.1 % is found with a 32 atom super-cell.

ficient for cell-size convergence. Since the calculations are most sensitive to the plane-wave cut off at lower temperatures, we performed the simulations at 10kK around the temperature of the lowest Hugoniot points calculated but high enough to provide a representative occupation of higher energy orbitals. The resolution of the plane-wave basis depends on the unit cell size. So, a separate test was performed for the two extreme densities considered here. The pressure rapidly converges with increasing plane-wave cut-off. Already at 200 eV cut-off we are nominally converged, and by 300 eV we are within the desired 1% accuracy. To be well converged, we chose a 340 eV which should provide results better than the 1% desired accuracy.

In Fig. 2, the pressure with respect to the number of atoms in the supercell is shown. The cut off was fixed at 340 eV and the temperature was set to 10kK. Convergence to within less than 1 % is rapidly achieved for a 32 atom supercell. Larger super cells provide very little increase in accuracy at a substantial computational cost.

Figure 3 portrays our calculated results, the high quality experimental data available, and two standardly used approximate models. We display only the AM05 GGA results so that the plot is less cluttered. The LDA curve is quantitative very similar but owing to a higher degree of complexity we might expect AM05 to perform more accurately. The boxes with error bars represent the results of gas gun experiments with an estimate of the experimental un-

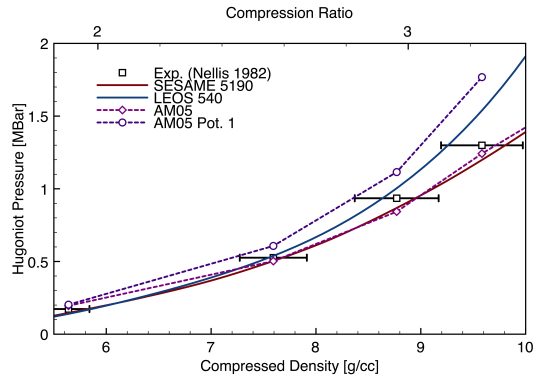


FIGURE 3. DFT-MD Hugoniot of shocked liquid Xenon using the AM05 GGA. Pot. 1 refers to the original pseudopotential that lacked proper description of f-shell phase shifts. Pot. 2 is the corrected pseudopotential. The solid lines are SESAME and LEOS equation of state models, and the squares with error bars represent the available gas gun data.

certainty. The error bars for the pressure measurement are smaller than the symbols while the density measurements are much more uncertain. It has been previously noticed that DFT-MD simulations when properly performed will lie safely within the error bars. However, the dashed curve with circles, which is our original result, generated using the first pseudopotential, lies outside the error bars especially at higher densities. Since we had shown that we were already converged with respect to cut-off and supercell size, a further problem was suspected. The number of calculated states was checked and shown to be sufficient to contain all electrons. Additionally, the electrons and nuclei had been treated on equal thermal basis. This led us to conclude that as the system grew hotter at higher pressure Hugoniot points, the physics was systematically described less accurately. This could be the case if the higher energy states were not treated properly in the pseudopotential. A reassessment of how the f-shell scattering was handled by the pseudopotential revealed that the potentials could be improved. The new improved potential did drastically effect the conclusions. The dashed curve with diamonds, the Hugoniot calculated with the new pseudopotential, is well within the experimental error bars and incidentally the plane-wave and supercell convergence slightly improved with the new pseudopotential. SESAME and LEOS

(solid lines) are empirical equation of state models and while both are clearly within the experimental margins, they are not consistent with each other. Since the DFT result lies close to the SESAME curve we might be tempted to conclude that the SESAME model is more accurate, but without tighter error bars on the experiment, this is hard to say with certainty.

Another observation is that it is important to include thermal occupation of the electronic states. The dashed curve is the result found when performing the simulation at fixed electron temperature of 163K and may be interpreted as an approximate Carr-Parinello treatment. Also shown is the Hugoniot curve that would result from theoretical calculations fixing the electrons to a cold temperature. Forcing cold electrons increases the pressure. Thus, the *cold* Hugoniot curve is much higher than the more accurate ones. In practice, the error may go unnoticed or perhaps compensated by other factors. Referring to our earlier convergence test, we see that not converging the plane-wave energy lowers the pressure. Thus, if we were to run cold electrons and low plane-wave cut-off, one can fortuitously get close to experimental at least over some range.

Figure 4 illustrates the density of the system in liquid insulator and metal phases. The liquid density is mostly non-overlapping and localized to the nuclei while in the metallic phase, the density is often shared between several ions. For the shock Hugoniot from liquid Xenon, we estimate the metal insulator transition pressure to be about 195 MBar ($T=6800\text{K}$) which is the first point calculated on our Hugoniot.

CONCLUSIONS

The importance of highly converged simulations cannot be over-estimated, DFT simulations are never better than numerical precision of the calculation. In this work, we have carefully tested convergence with respect to the energy cut off by requiring that both pressure and energy are converged within 1 %. The simulations were run long enough to ensure statistical uncertainties are smaller than the error introduced by a finite energy cut off. We used 1 mean-value point, an approximation that is known to be reliable. Our calculations were carefully compared to available experimental data allowing us to identify certain shortcomings of the PAW potentials. The

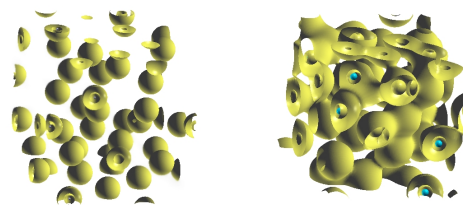


FIGURE 4. DFT-MD electron iso-density surface for liquid insulating and liquid metallic Xenon. On the left is an intermediate density from a supercell of insulating liquid xenon with molar volume 44.21 cc/mol or density 2.696 g/cc at 163 K. The more extended iso-density to the right is from the metallic higher density and temperature phase with molar volume 11.054 cc/mol or density 11.877 g/cc at $T=80\text{ kK}$.

resulting analysis predicts a Hugoniot curve is in excellent agreement with experiment and the SESAME 5190 EOS.

ACKNOWLEDGMENTS

Sandia is a multiprogram laboratory operated by Sandia Corporation, a Lockheed Martin Company, for the United States Department of Energy's National Nuclear Security Administration under contract DE-AC04-94AL85000.

REFERENCES

1. Mikhailova, O., Mochalov, M., Sokolova, A., and Urlin, V., *High Temperature*, **38**, 210–214 (2000).
2. Worth, J., and Trickey, S., *Phys. Rev. B*, **19**, 3310 (1979).
3. Shindo, K., and Nishikawa, A., *Journal of the Physical Society of Japan*, **60**, 3579–3580 (1991).
4. Reichlin, R., Brister, K., McMahan, A., Ross, M., Martin, S., Vohra, Y., and Ruoff, A., *Phys. Rev. Lett.*, **62**, 669 (1989).
5. Militzer, B., <http://arxiv.org/abs/0805.0317v1> (2008).
6. Chen, Q. F., Cai, L. C., Gu, Y. J., and Gu, Y., *Phys. Rev. E*, **79**, 016409 (2009).
7. Nellis, W., v. Thiel, M., and Mitchell, A., *Phys. Rev. Lett.*, **48**, 816 (1981).
8. Belonoshko, A. B., Davis, S., Rosengren, A., Ahuja, R., Johansson, B., Simak, S. I., Burakovsky, L., and Preston, D. L., *Phys. Rev. B*, **74**, 054114 (2006).

9. Ross, M., Boehler, R., and Soderlind, P., *Phys. Rev. Lett.*, **95**, 257801 (2005).
10. Desjarlais, M. P., *Contrib. Plasma Phys.*, **45**, 300 D 304 (2005).
11. Sifner, O., and Klomfar, J., *J. Phys. Chem. Ref. Data*, **23**, 63 (1994).
12. Hohenberg, P., and Kohn, W., *Phys. Rev.*, **136**, B864 (1964).
13. Kohn, W., and Sham, L. J., *Phys. Rev.*, **140**, A1133 (1965).
14. Mattsson, A. E., Schultz, P. A., Desjarlais, M. P., Mattsson, T. R., and Leung, K., *Modelling Simul. Mater. Sci. Eng.*, **13**, R1 (2005).
15. Kresse, G., and Hafner, J., *Phys. Rev. B*, **47**, R558 (1993).
16. Kresse, G., and Hafner, J., *Phys. Rev. B*, **49**, 14251 (1994).
17. Kresse, G., and Furthmüller, J., *Phys. Rev. B*, **54**, 11169 (1996).
18. Blöchl, P. E., *Phys. Rev. B*, **50**, 17953 (1994).
19. Kresse, G., and Joubert, D., *Phys. Rev. B*, **59**, 1758 (1999).
20. Mermin, N., *Phys. Rev.*, **137**, A1441 (1965).
21. Mattsson, T. R., and Desjarlais, M. P., *Phys. Rev. Lett.*, **97**, 017801 (2006).
22. Armiento, R., and Mattsson, A. E., *Phys. Rev. B*, **72**, 085108 (2005).
23. Mattsson, A. E., Armiento, R., Paier, J., Kresse, G., Wills, J. M., and Mattsson, T. R., *J. Chem. Phys.*, **128**, 084714 (2008).